

2. Research and Developments at the PF Storage Ring

2-1. Photon Beam Position Monitor System in the Frontends

A photon beam-position monitor system is installed in the frontends to monitor the stability of the photon beams. The monitor heads are photo-emission types, which consist of a pair of triangular blades. A photograph of the monitor head is shown in Fig. 1. The locations of the monitors are summarized in Table 1. We separate the monitor heads into four groups. The group has monitors in one quarter of the ring. Four stations for them have the data acquisition systems that are assigned for each group of the monitor heads. The data-acquisition system consists of a current amplifier and a difference circuit to evaluate the photon beam position. All analog data of the photon beam positions are sent to the control room for recording and further analysis. The analog data of the photon beam positions are recorded and converted into digital data using a digital recorder. Converted digital data are relayed to a computer in the control room for display and further analysis. A block diagram of the data-acquisition system is shown in Fig. 2. The photon beam positions are displayed on a CRT in the con-

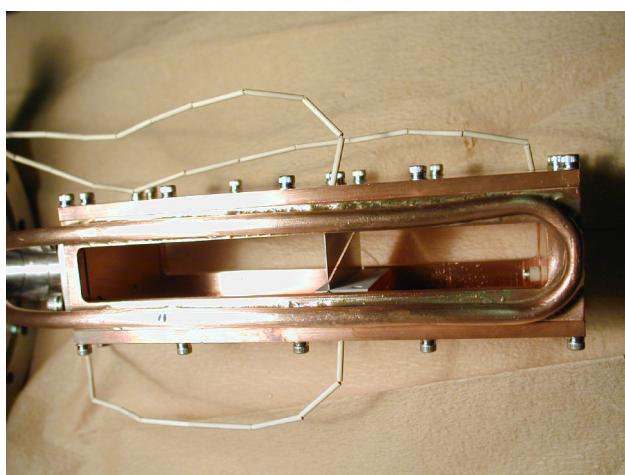


Figure 1.
A photograph of the monitor head.

Table 1.
The locations of the monitors.

station	beamline number	position [mm]
1	BL-4	4925
	BL-6	4275
	BL-7	4300
	BL-8	4300
2	BL-9	4300
	BL-10	4300
	BL-11	4275
	BL-12	4300
3	BL-18	5690
	BL-20	4185
4	BL-27	9190
	BL-1	4300

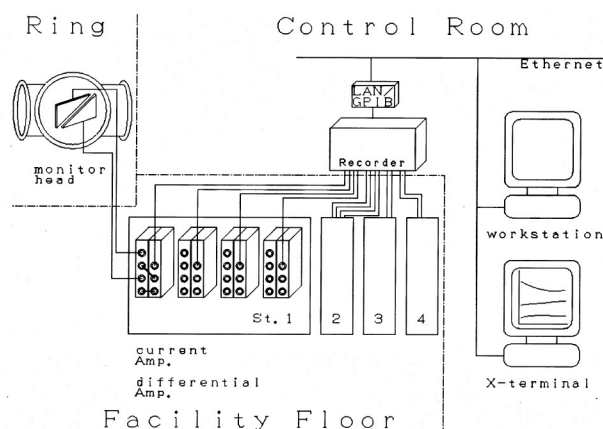


Figure 2.
Block diagram of the data acquisition system.

trol room. The display panel is shown in Fig. 3. The photon beam positions are displayed every two seconds and for a 30-min span; 24-hour movements of the photon beam positions are also displayed in the panel. We can calibrate the monitors automatically by a computer in the control room.

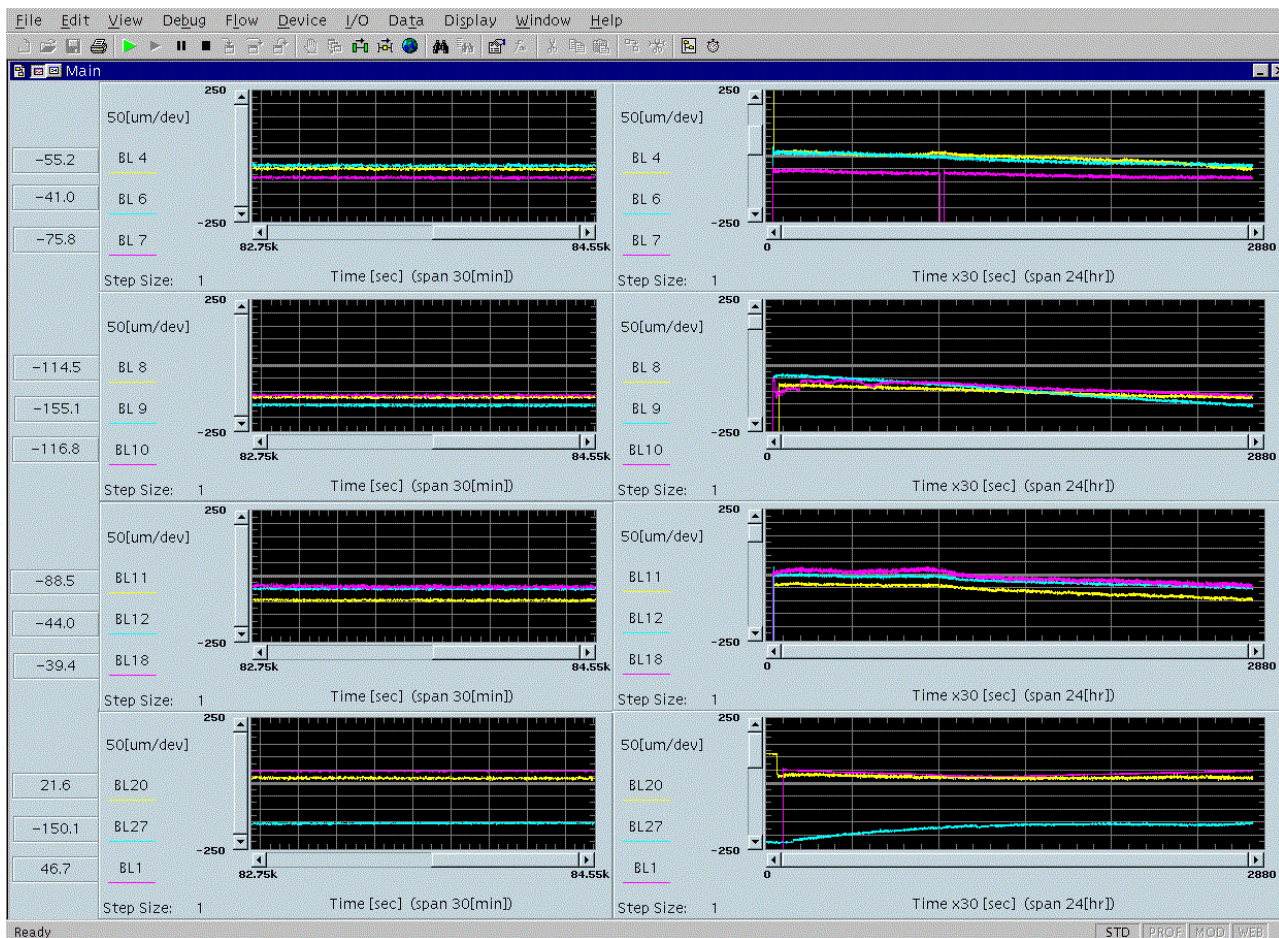


Figure 3.
The display panel for photon beam positions.

2-2. Beam-Based Alignment of the Beam-Position Monitors

The offsets of the beam-position monitors (BPM) have been examined using a stored electron beam. The origin of the BPM is defined as the magnetic center of the adjacent quadrupole magnet. At the construction stage, the electrical center of each BPM was calibrated on a test bench, and the monitor head was mechanically aligned to the quadrupole's center. The total error on the BPM center was declared to be a few hundred μm . We measured the vertical offsets for all BPMs and detected an offset drift which occurred at a specific BPM.

An electronic load-switch system has been prepared for measuring the lattice parameters. One of the quadrupole magnets is selected and its current

can be changed independently. For the beam-based alignment, we controlled the electronic load by using an external oscillator. The current of a quadrupole magnet was typically altered by an amplitude of 3 A and by a frequency at 5 Hz. In this condition, an orbit oscillation of a few μm in amplitude occurred. The oscillation was detected by a BPM in another portion from the specified quadrupole. The 5-Hz component of the orbit oscillation could be measured using an FFT analyzer with sufficient stability and sensitivity. A local bump was prepared for the pair of quadrupole magnets and the nearest BPM. When the amplitude of the orbit oscillation was plotted as a function of the BPM readings, we obtained the graph as shown in Fig. 4. In Fig. 4, the local bump was created in the vertical direction. We could draw two straight lines that linked the data points. The

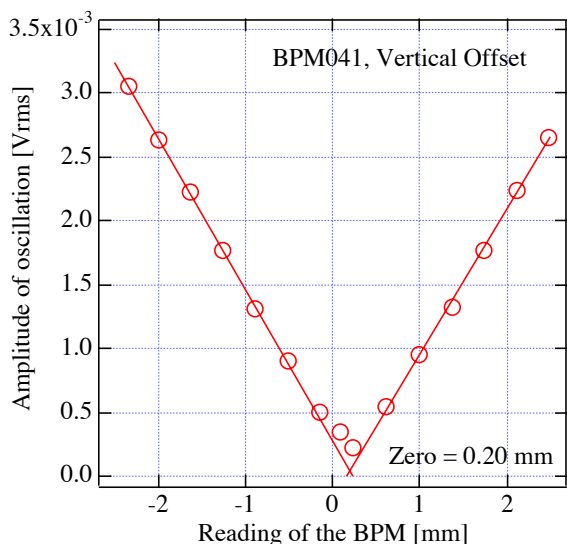


Figure 4. Measurement of the BPM offset.

two lines crossed near the bottom axis. The slopes of both lines were symmetric about the intersection. The intersection was assumed to be an orbit at the center of the magnetic field. Thus reading of the BPM at the intersection was offset to the magnetic center.

In Fig. 5, vertical offset data for all the BPMs are plotted. Among a total of 65 BPMs, 42 are 4-button

BPMs which were installed during the last low-emittance reconstruction in 1997. The other BPMs that remain in straight sections are 6-electrode type. Two histograms for each type of BPM are shown in Fig. 6. For the 4-electrode BPMs, the offsets are distributed almost symmetrically around zero, and the standard deviation is estimated to be 0.47 mm. In the central part of Fig. 5, which is one of the insertion-device sections, there is a remarkable hill of over +1 mm. Such a systematic error is predominant among the 6-electrode BPMs. It can be seen in the histogram for the 6-electrode BPM that the center of the distribution obviously shifts to a positive offset.

The drift of the BPM offset was practically detected as a function of the beam current by a beam-based measurement. In a single-bunch mode, the vertical beam positions at a few BPMs could not be aligned to the reference orbit by the usual COD correction procedure. The BPM, called “283” is one of such BPMs. When a rather high current was stored in a single bunch, some portions of the vacuum duct suffered from heating. Also, in the 3-GeV operation, the vertical position at the BPM283 protruded from the reference orbit line. We thus

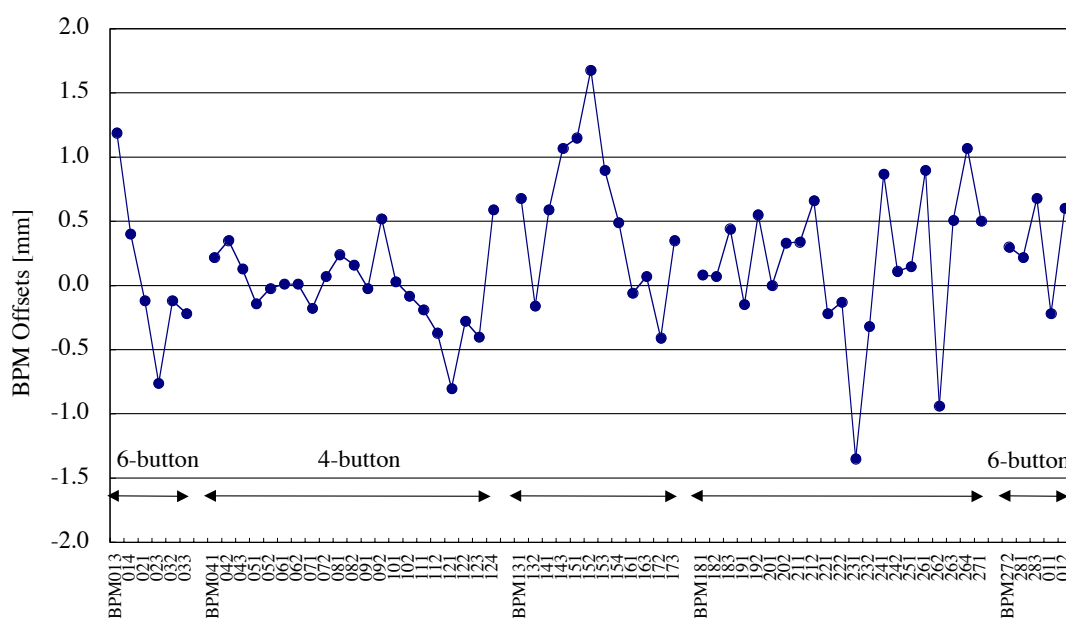


Figure 5. Vertical offsets of all the BPMs. The positions of the BPMs are shown in the figure on p. 111.

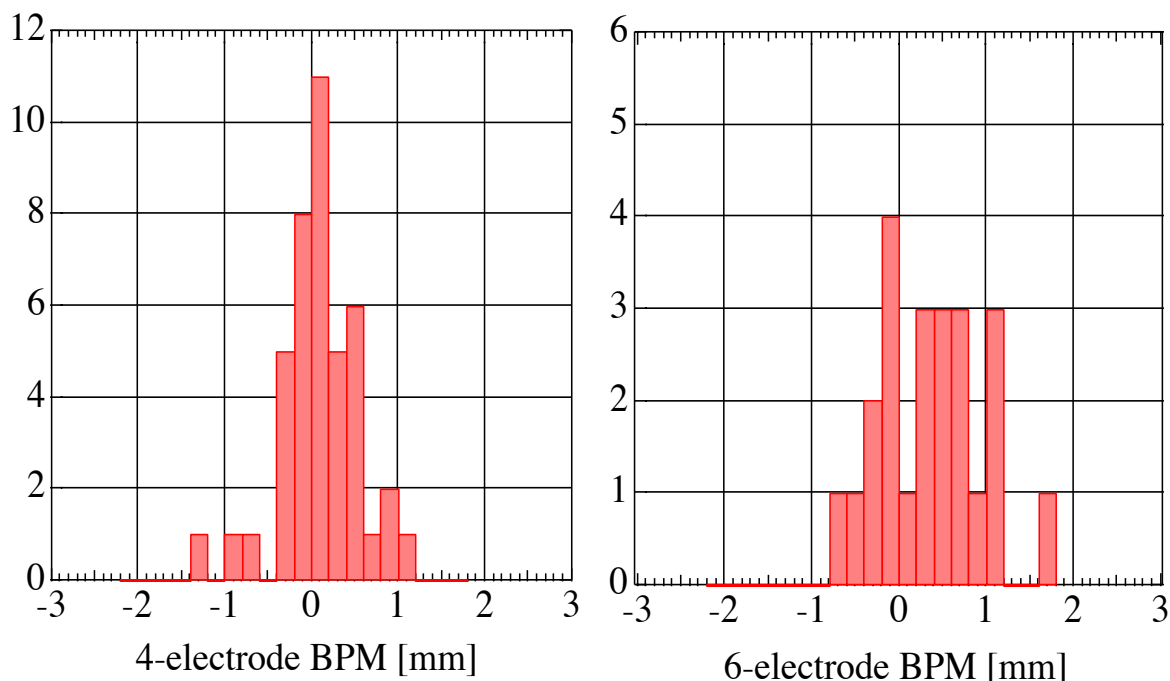


Figure 6.

Histogram of the BPM offsets: left) 4-electrode BPMs; right) 6-electrode BPMs.

speculated that a few BPMs, including the BPM283, had an offset drift depending on the temperature change. In Fig. 7, the current dependence of the offset is shown along with the data for BPM281. Both BPMs are of the same type, and are installed at both sides of a triplet of quadrupoles. It is clear that the BPM283 did drift by as much as 0.3 mm under a high current. On the other hand, it is also clear that the BPM281 did not suffer from any drift. The beam positions at most of the BPMs could be aligned to a reference orbit by an ordinary COD correction. The number of BPMs that suffer from the offset drift would not be very large.

In summary, the vertical offsets of most of the BPMs were better than ± 0.5 mm, though some BPMs had undesirable offsets of over 1 mm. Especially at some portions of the straight sections, a systematic error was discovered. The drift of the BPM offset could be revealed by a beam-based measurement. We plan to specify which BPM has an offset drift like the BPM283. This will be useful to improve the performance of orbit stabilization.

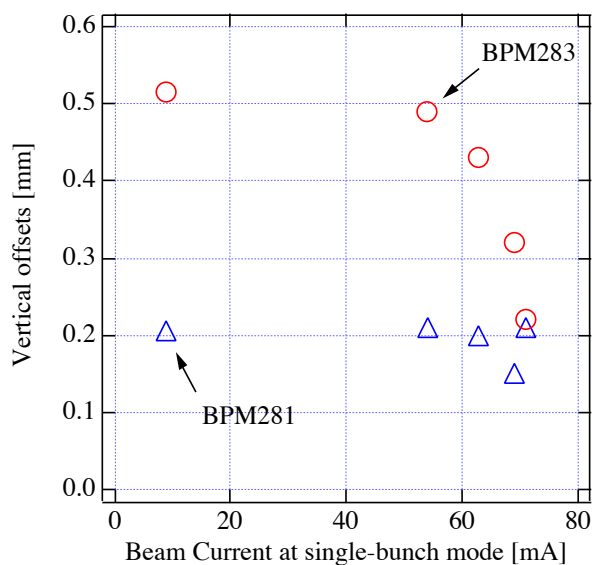


Figure 7.

Variation of the vertical offset as a function of the beam current observed at a specific BPM (under single-bunch operation).

2-3. Longitudinal Bunch Oscillations Induced by RF Phase Modulation

In order to improve the beam lifetime under daily operation, an rf phase-modulation method [1,2] has been used since May, 1999. In this method, bunch-length oscillation is induced by modulating the rf phase at a frequency close to two-times the synchrotron frequency. This results in a long bunch length and, thus, in a long Touschek lifetime.

In order to investigate the beam behavior under this modulation, we observed induced bunch oscillations [3] under single-bunch operation. Figure 8 shows the longitudinal bunch oscillations, which were measured by detecting the visible synchrotron light with a dual-sweep streak camera. The longitudinal bunch profile is shown along the vertical axis, while its slow variation is shown along the horizon-

tal axis. The data under no modulation are shown in Fig. 8(a). When we applied phase modulation with a peak-to-peak amplitude of 8° at a frequency of 40.2 kHz (about 3 kHz lower than a frequency of $2f_s$, where f_s is the synchrotron frequency at low currents), a single bunch split into three bunchlets, as shown in Fig. 8(b). Two of them played synchrotron oscillations having opposite phases, while the other bunchlet stayed almost still. Next, when we increased the modulation frequency by 0.4 kHz, the particle population in the center bunchlet decreased, as shown in Fig. 8(c). Finally, when we increased the frequency further by 0.3 kHz, the center bunchlet became faint. Note that the rf voltage during this experiment was about 1.4 MV and that the coherent synchrotron frequency was about 21.6 kHz.

The above-mentioned observations were compared with the simulation results. Some of the results

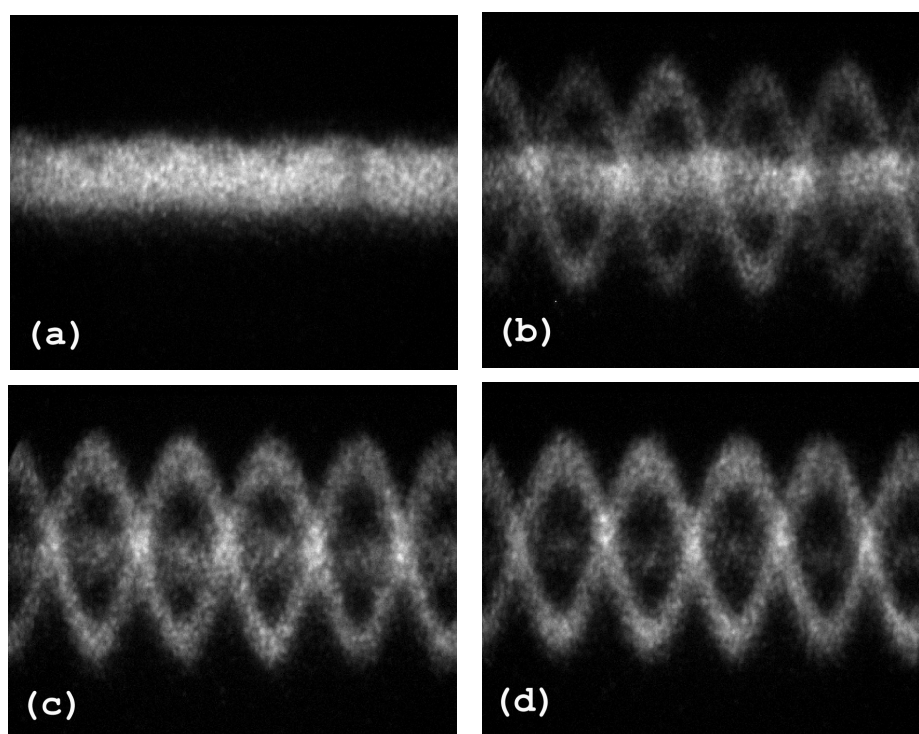


Figure 8.

Measured longitudinal oscillations of a single bunch [3]. Images from a dual-sweep streak camera were shown. A longitudinal profile of the bunch is shown along the vertical axis (1 ns full scale), while its slow variation is shown along the horizontal axis (100 ms full scale). (a) Without any modulation. In the cases of (b)-(d), phase modulation was applied with a frequency of: (b) 40.2 kHz, (c) 40.6 kHz, and (d) 40.9 kHz, respectively. The beam currents were 31-28 mA.

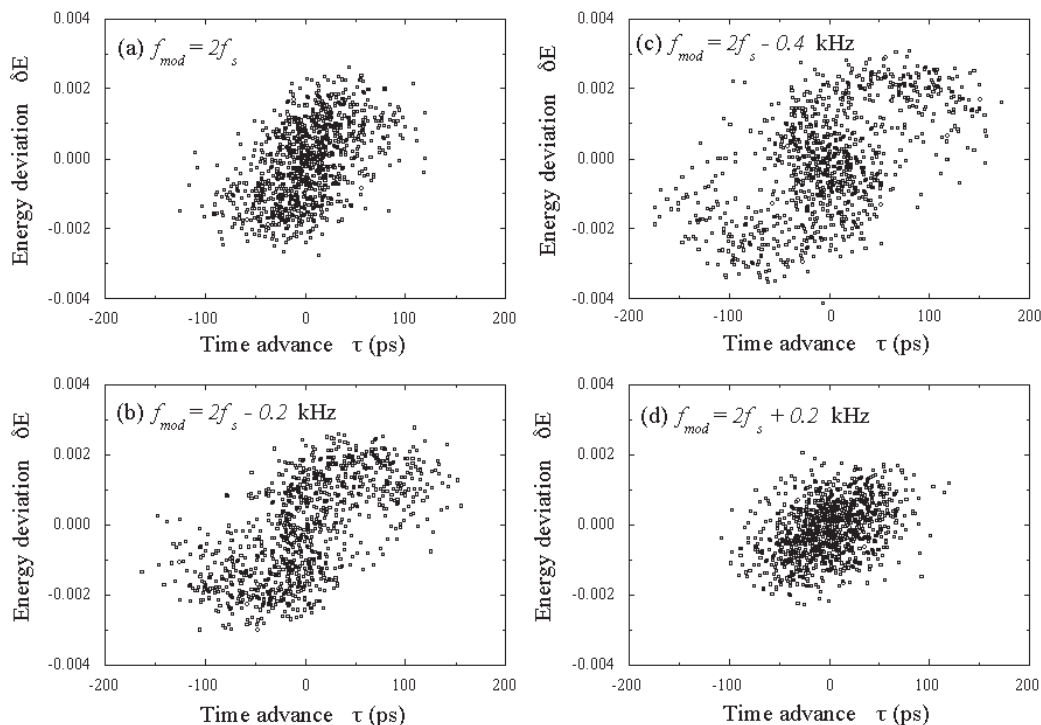


Figure 9.

Result of tracking simulations [3]. A single bunch was modeled with 1000 macro-particles. The phase-space distributions of the particles after about 6×10^4 turns are shown. The assumed phase-modulation amplitude is 8° p-p and the beam current is 30 mA. Figures (a) - (d) correspond to different modulation frequencies, which are shown in the figures. Note that a frequency of $2f_s$ was about 40.87 kHz in this calculation.

of a multi-particle tracking simulation are shown in Fig. 9. It can be seen from Figs. 9(a) and 9(b) that two groups of particles (bunchlets) were formed when the modulation frequency was close to a frequency of $2f_s$. When the modulation frequency was slightly lower, on the other hand, three groups were formed, as shown in Fig. 9(c). These simulation results qualitatively agree with the above observations. These results are also consistent with a theoretical analysis on a single-particle motion.

References

- [1] S. Sakanaka, M. Izawa, T. Mitsuhashi, T. Takahashi, *Phys. Rev. ST - Accel. Beams* 3 (2000) 050701.
- [2] Photon Factory Activity Report #17 1999 PART-A (2000) 121.
- [3] S. Sakanaka and T. Obina, *Jpn. J. Appl. Phys.* 40 (2001) 2465.

2-4. Measurement of Third-Order Resonance Islands

The nonlinear beam dynamics of the transverse betatron motion in a circular accelerator has been studied using analytical, numerical and experimental methods. Despite progress in explaining of nonlinear phenomena, there is still a gap between the analytical studies, numerical prediction and reality. Especially, perturbation theory is limited near to a resonance. To reduce this gap, experimental nonlinear-beam-dynamics studies have become increasingly important. We have experimentally studied the phase-space topology near the resonances using a transverse phase-space monitor system [1].

In the PF ring, to suppress transverse instabilities, four octupole magnets are installed. The octupole magnets can produce a large amplitude-dependent tune shift to the beam. The effect near a res-

onance has attracted considerable interest. This report concerns the study of phase-space topology under various octupole-field strengths near the third-order resonance.

The phase-space monitor system consists of fast kicker magnets and turn-by-turn monitors [2]. The fast kicker magnets provide beams with a large coherent motion. The coherent betatron motion was measured until 16,384 turns by using turn-by-turn monitors. To measure the coherent betatron motion in phase space, two BPMs at a long straight section are used. The beam position (y) and the beam angle y' are obtained from data at the two positions.

The experiment was performed in the single-bunch operation mode. The initial stored current was set to be about 5 mA. To measure the vertical coherent betatron motions near the third-order resonance line ($3\nu_y = 13$), the initial betatron tunes were selected near $(\nu_x, \nu_y) = (9.60, 4.33)$. The typi-

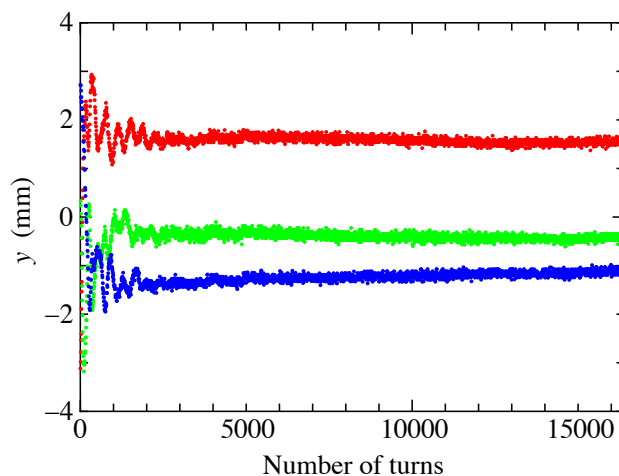


Figure 10.

Vertical coherent betatron motion measured at an octupole excitation current of -1.0 A shown as a function of turn. The red, green and blue dots correspond to the data for $(3i-2)$, $(3i-1)$ and $3i$ turns, respectively, where $i = 1, 2, \dots$

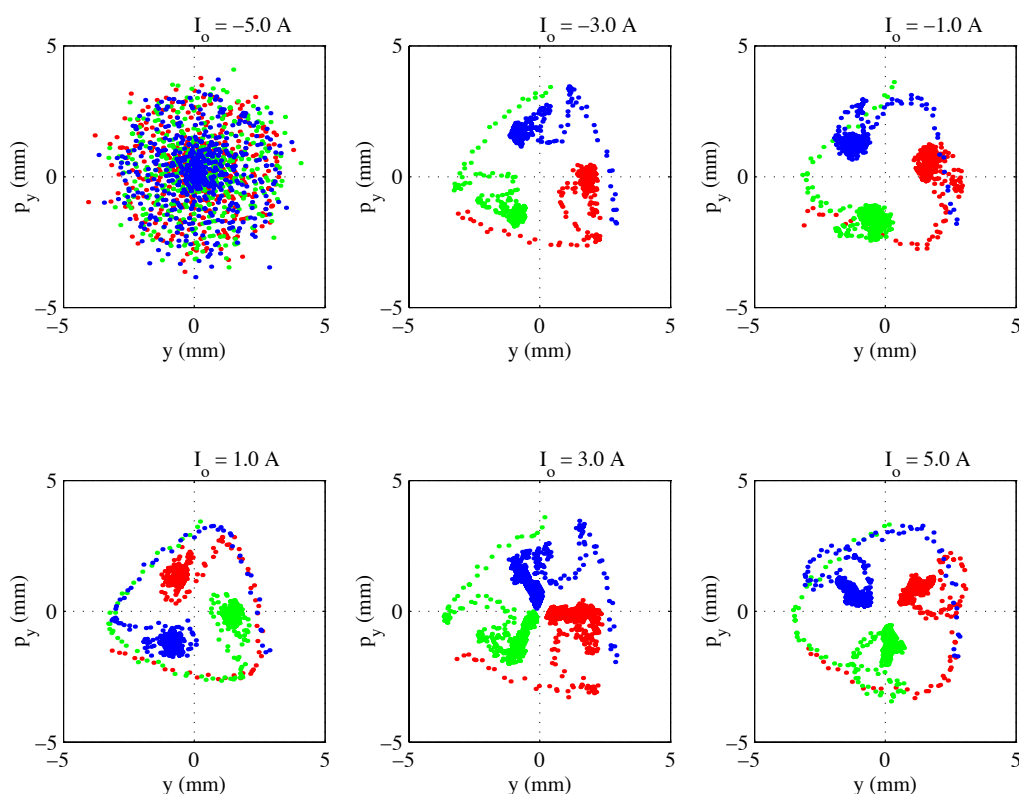


Figure 11.

Poincaré map for motion near the third-order resonance for six different octupole excitation currents: -5.0 , -3.0 , -1.0 , 1.0 , 3.0 and 5.0 A. p_y is normalized momentum, which is calculated by using y , y' and Twiss parameters.

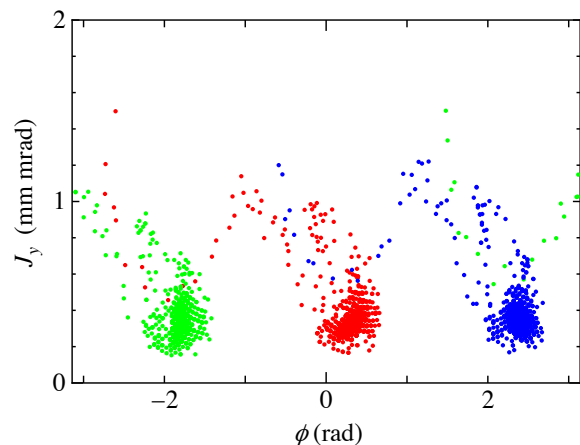


Figure 12.

Poincaré map in action-angle variables for particles trapped in a third-order resonance island at an octupole excitation current of -1.0 A.

cal result of an experiment in which the particles were trapped in the third-order resonance island, is shown in Fig. 10.

In order to search a condition in which the particles are trapped in the resonance islands, we changed the initial betatron tunes and the vertical amplitude. Under many experimental conditions, the particles were not trapped in the island, and the coherent motions were damped. At a particular condition, the particles were trapped in the island. This condition was very sensitive to the initial betatron tunes and the vertical amplitude.

Figure 11 displays a vertical phase-space plot (Poincaré map) for six different octupole excitation currents. When the octupole excitation current was more than -3.0 A, the particles were trapped in the island. The motion in the phase space depended on the octupole excitation current. The data shown in Fig. 11 are plotted in J - ϕ space in Fig. 12. J_y is introduced as the position of the third-order resonance island, which is an average of the action (J_y) from 9,000 turns to 10,000 turns. That is the reason why the J_y approached a constant value after 9,000 turns. Figure 13 shows the average action ($\langle J_y \rangle$) as a function of the octupole excitation current (I_o). As shown in Fig. 13, $\langle J_y \rangle$ was not constant, and was

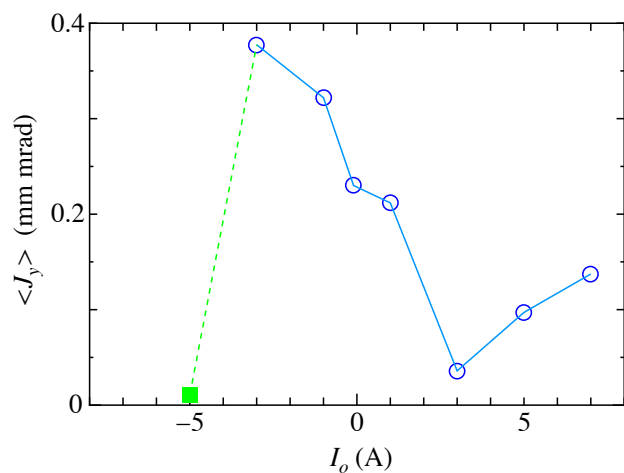


Figure 13.

Average action J_y for the particles trapped in third-order resonance island for eight different octupole excitation currents: -5.0 , -3.0 , -1.0 , -0.1 , 1.0 , 3.0 , 5.0 and 7.0 A. For $I_o = -5.0$ A the particles were not trapped in the island. For $I_o = 7.0$ A slight beam loss was observed.

minimum at $I_o = 3.0$ A.

In this experiment, the coherent motion after a vertical kick was examined with various field strengths of the octupole magnets near the third-order resonance line. We guess that the dependency of the motion in the resonance island is generated by a slight difference of the amplitude dependent tune shift due to the octupole magnets. We are now going to better understand the phenomena through detailed theoretical and numerical approaches.

References

- [1] T. Miyajima et al., in *Proceedings of the 2001 Particle Accelerator Conference, Chicago, 2001* (to be published).
- [2] Y. Kobayashi et al., in *Proceedings of the Fifth European Particle Accelerator Conference, 1996*, pp. 1666.

2-5. Ion-Related Vertical Instability

In the PF ring, a vertical instability has been observed during a multi-bunch operation in which a series of 280 bunches followed by a series of 32 empty buckets is stored [1]. The instability can be suppressed by the excitation of octupole magnets in routine operation; however, the phenomenon has not been sufficiently characterized up to now.

The instability depends on the vacuum condition in the ring: namely, the instability is enhanced under poor vacuum conditions and improved under good vacuum conditions; this fact implies that the phenomenon is ion-related. The ions are attracted and trapped by the electron beam and, consequently, the beam passes through “ion-clouds”. The beam is affected by the Lorentz force due to the ion-clouds, and the original motion of the beam can be affected. This phenomenon is called an ion-trapping effect, and can cause a tune shift.

We measured the vertical tunes of individual bunches in the multi-bunch operation by observing spontaneous betatron oscillation using an optical bunch-by-bunch beam-diagnostic system [2] installed

in BL-21. A schematic diagram of the beam-diagnostic system is shown in Fig. 14. A pockels cell is placed between polarization filters whose polarization angles are perpendicular to each other. The incident light can pass through the vertical polarizer while a high-voltage pulse is applied to the cell, because it rotates the polarization plane. A high-voltage pulser generates pulses with a height of 550 V and a width (FWHM) of about 1.5 ns, which is shorter than a bunch spacing of 2 ns.

Light through the shutter is focused by a lens to form an image of the beam on a horizontal edge that cuts off half the image. The intensity of the light through the edge is detected by a photomultiplier tube (PMT). The vertical motion of the beam can be detected as an amplitude variation of the output signal of the PMT. The output signal of the PMT is analyzed with a spectrum analyzer.

Figure 15 shows the measured tune shifts from the tune of the first bunch as a function of the bunch position in the bunch train. It is clearly seen that the tunes depend on the position in the bunch train and, especially, that the tunes gradually increase along the bunch train in the head and decrease again in

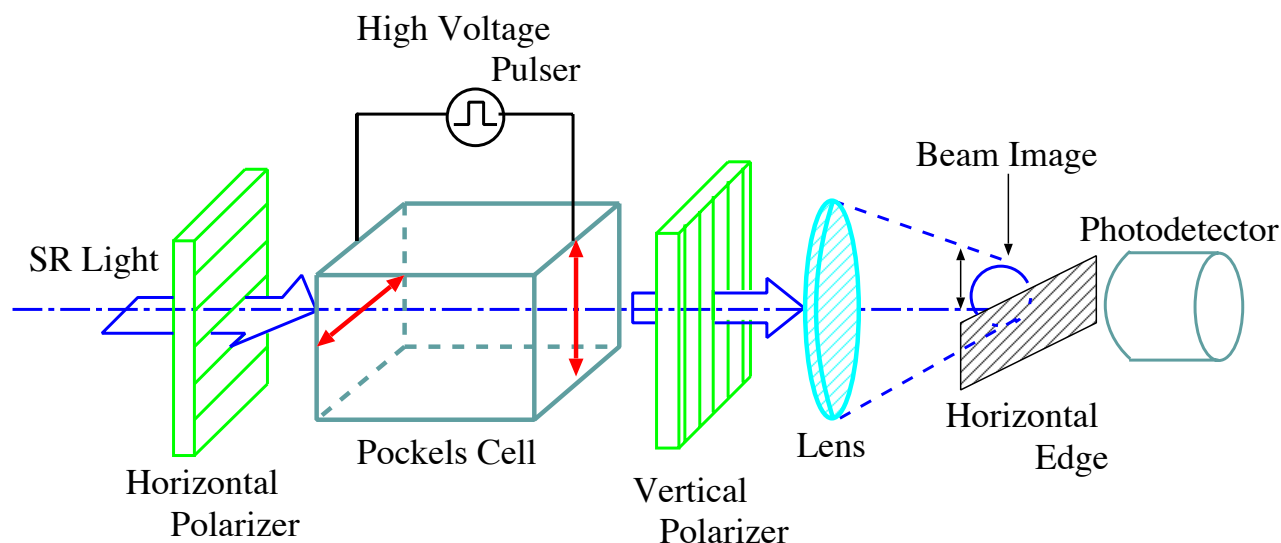


Figure 14.

Schematic diagram of the optical bunch-by-bunch beam-diagnostic system.

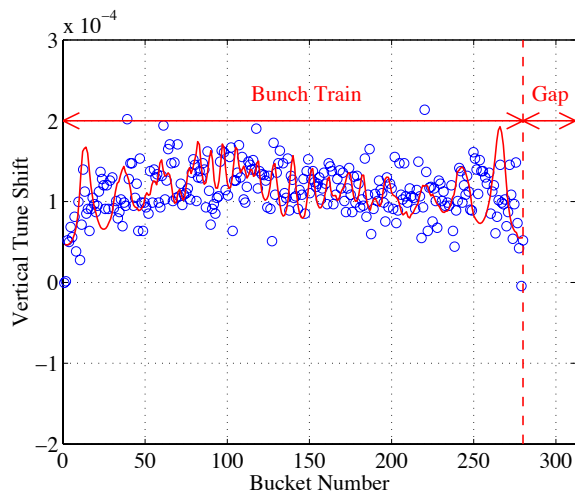


Figure 15.

Change in the tunes along a 280-bunch train. The blue circles and the red curve correspond to the experimental results and the theoretical values, respectively.

the tail. The change in the tunes along 20 successive bunches in the head of the train is estimated to be 4.0×10^{-6} /bunch. This is more than 10-times as large as the estimated value from the FBII theory [3] under the same conditions. In the theoretical calculation, ion species of CO^+ is assumed because it is a main component of residual gas in the PF ring. A pressure of 75 nPa for the CO is assumed around the beam orbit. It is 3-times as large as the measured partial pressure of the CO where the gauges are set [4].

In order to explain the dependence of the tunes on the position in the bunch train, we considered the motion of trapped ions by a method similar to the theory of betatron oscillation in circular accelerators, and calculated the change in the size of ion-clouds due to the passage of a bunch train. We estimated the change in the vertical tunes along the bunch train due to the modulation of the ion density along the train [5]. The theoretical value of the change in the tunes along the train for CO^+ ion is also shown in Fig. 15. The averaged tune shifts along 20 bunches in the head and the tail are estimated to be 5.1×10^{-6} /bunch and -6.4×10^{-6} /bunch, which agree well

with the experimental values.

We have improved the mirror system in BL-21 and increased the photon flux for the beam-diagnostic system for more precise measurements. A further development of an optical beam-diagnostic system, that can detect both the betatron tunes and the oscillation amplitudes of individual bunches simultaneously, is also being planned.

References

- [1] Photon Factory Activity Report #17 1999 PART A (2000) 124.
- [2] A. Mochihashi, et al., to be printed in Proc. the 5th European Workshop on Diagnostics and Beam Instrumentation, Grenoble (2001).
- [3] T. O. Raubenheimer and F. Zimmermann, Phys. Rev. E 52 (1995) 5487.
- [4] Y. Hori (private communication).
- [5] A. Mochihashi et al., Phys. Rev. ST Accel. Beams 4 (2001) 022802.

2-6. Radiation Experiments at BL-21

BL-21 has two kinds of beamlines. One is used for our studies on the material characteristics with SR irradiation. The results can be applied to some accelerators to improve their current conditions, or to develop new vacuum devices. We carried out two kinds of irradiation experiments at the BL-21 vacuum line, as follows:

(a) *Researching properties of photon-stimulated electrons (photoelectrons) with the aim of obtaining some effective solutions to a serious problem in the KEK B-Factory positron storage ring (KEKB-LER).*

One of the most serious problems in the KEKB operation has been vertical beam size blow-up of the positron beam, which has been limiting the luminosity of KEKB as an electron-positron collider [1]. This phenomenon is now considered to be due to the single-beam instability caused by the electron

cloud around the beam; its source is mainly photoelectrons from the OFC (Oxygen Free Copper) vacuum ducts. To find some effective solutions to this issue, the vacuum group staff of KEKB, SRRRC (Synchrotron Radiation Research Center in Taiwan) and KEK-PF simulated a part of the KEKB vacuum ducts by installing a 300 mm-long copper chamber at BL-21, where SR (Synchrotron Radiation) with a critical energy (E_c) of 4 keV hits the inside of the

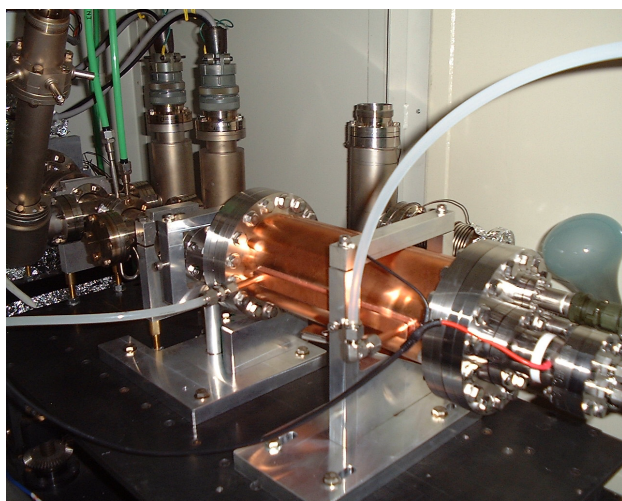


Figure 16.
Test chamber installed at the end of BL-21 vacuum line.

chamber at an incident angle of 3° . Sixteen electrodes arranged inside the chamber provide some useful information about photoelectrons, such as the spatial distribution as well as the photoelectron yield.

At first, we irradiated a test chamber whose inside surface was machined like a saw-tooth, and measured the photoelectron intensity around the center of the chamber, where the positron beams are supposed to pass through. It was known that the saw-tooth surface was effective to reduce the photoelectron yield for the SR with a low critical energy of several tens eV in past experiments at CERN. But, we needed to know how effective this method would be in the keV region, because the critical energy of KEK-LER is 6 keV. Our result also showed that the photoelectron yield was reduced by 94% compared to the actual smooth surface [2]. To see the validity in the presence of a positron beam, a 2.6 m-long test chamber with a shallow saw-tooth surface will be installed in the KEKB-LER during the summer of 2001.

Secondly, we examined the effect of a magnetic field from permanent magnets or a solenoid coil

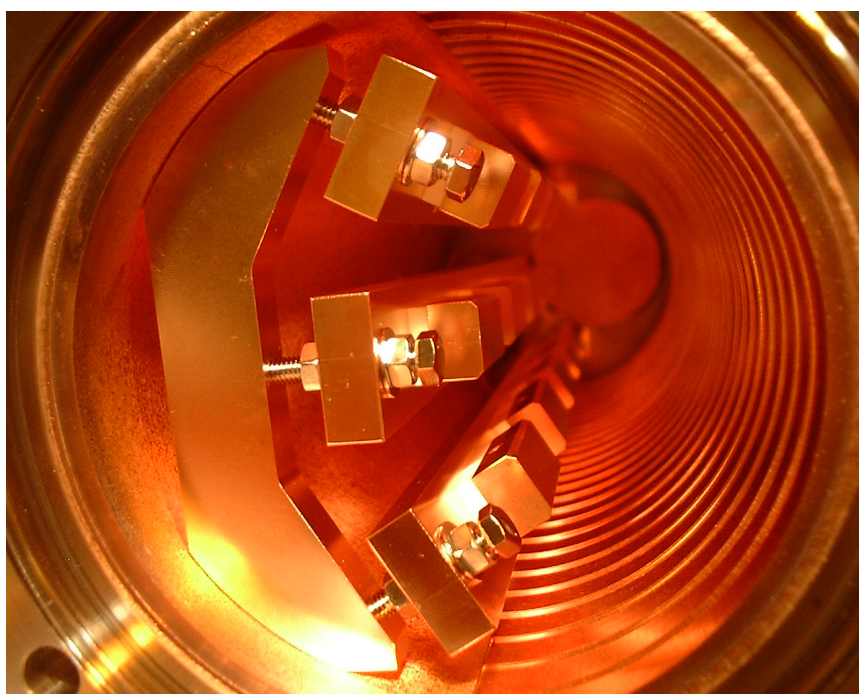


Figure 17.
Inside of the test chamber.
Sixteen electrodes pick up the photoelectrons. The SR hits the right-hand surface, which was machined like a saw-tooth.

upon the photoelectron intensity around the center of the test chamber. This experiment revealed that a uniform field of the solenoid coil was more effective, and a magnetic field larger than 50 Gauss could reduce the intensity of the photoelectrons by 90% [3]. Actually, the solenoid coil method has been applied to the KEKB-LER, which contributed toward increasing the luminosity.

References

- [1] H. Fukuma et al., *Proceedings of EPAC2000*, Vienna, 1122.
- [2] Y. Suetsugu et al., *Proceedings of PAC2001*, Chicago, to be published.
- [3] Y. Suetsugu et al., *Proceedings of PAC2001*, Chicago, to be published.

(b) Testing a new photon absorber for the planning Shanghai Synchrotron Radiation Facility (SSRF)

This experiment was performed as part of an academic interchange in the core university system among some universities in China and KEK-PF. Using the BL-21 vacuum line, a prototype of a copper absorber for the SSRF project was tested

by measuring the photon-stimulated gas desorption (PSD) from both the absorber and the aluminum chamber wall during SR irradiation.

We measured the SR dose dependence of the PSD during 2.5-GeV and 3.0-GeV operation, and also after the N₂ glow discharge cleaning process in the test chamber. Especially the glow discharge method was found to be useful in this kind of circumstance because it could reduce the PSD by 50% after an accumulated SR dose of 15A-h. Although the SR energy at KEK-PF ($E_c \sim 7$ keV at 3.0 GeV operation) was not the same as that at SSRF ($E_c \sim 10$ keV), we obtained a prospect for the future use of this kind of absorber based on the result of this experiment.

2-7. Bunch-Length Measurement by Second-Order Autocorrelation

The bunch length is one of the fundamental beam parameters in the storage ring. Since the typical bunch length is a few tens of ps, it is very difficult to measure by the electric method. Because a

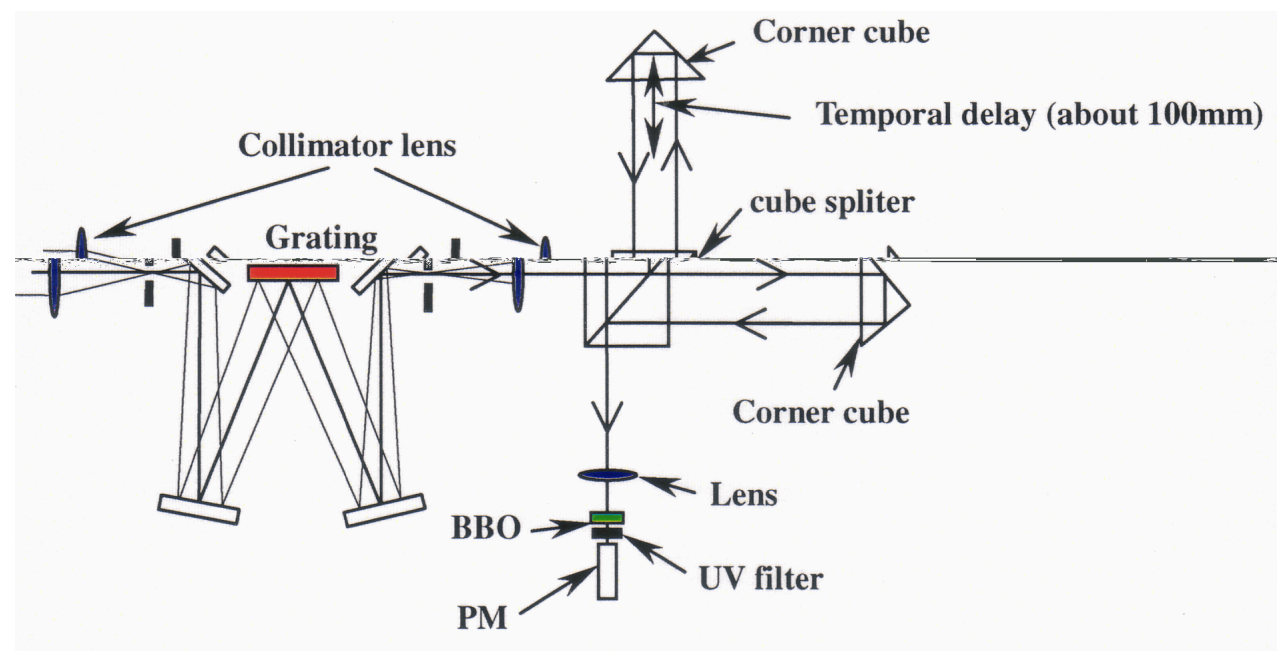


Figure 18.
The setup of autocorrelator with colinear arrangement.

streak camera has a good temporal resolution in the ps range, we usually use this apparatus for bunch-length measurements. The temporal resolution of a streak camera is related to the spatial electron or the photon profile, and is limited to light pulses longer than a few hundred fs. Recently, the development of ultrashort electron pulses (100-fs range) has been undertaken in some facilities, such as the FEL facil-

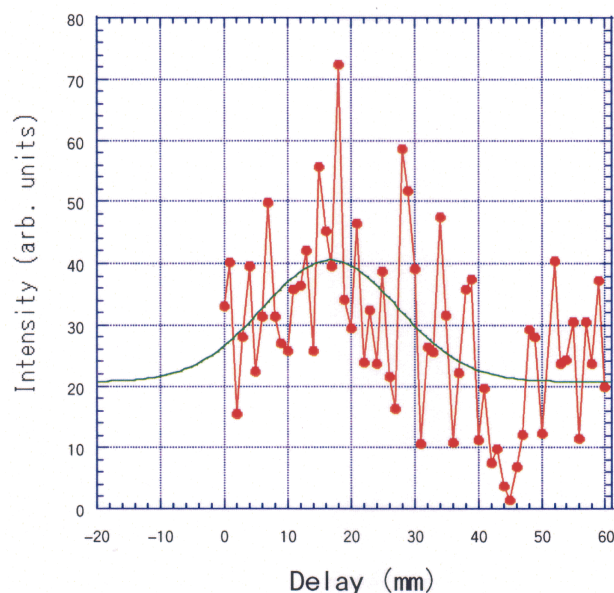


Figure 19. Result of an intensity autocorrelation trace for an electron bunch at the PF ring.

ities. In optical science, we usually use the second-order autocorrelation method to measure the ultra-short pulse length. This method can measure those light pulses that are non-Fourier transfer limited pulses, and having a good temporal resolution down to the fs range. At this moment, we are trying to demonstrate that this method is also available for measuring the bunch length. The basic experimental setup is shown in Fig. 18. The design of the autocorrelator is based on the currently-used colinear arrangement. Since the coherent length is too short with the white beam, we applied a monochromator to limit the bandwidth of 10^{-4} at the wavelength of 633 nm. We used a nonlinear crystal BBO (β -Barium Borate) with type I phase matching arrangement to obtain the SHG signal. The measurement was performed at optical monitor in the BL27 (bending source). The ring was operated under a single-bunch mode and the beam current was 30 mA. A result of intensity autocorrelation trace is shown in Fig. 19. Due to the interference fringe (first order) in the colinear arrangement, the data points are fluctuated, but we can see the bunch envelope. To evaluate the bunch length, we fit a Gaussian profile, and result is 15 mm. This result is agreed with a result from the streak camera measurement.